Hierarchical Porous Nitrogen-Doped Carbon Nanosheets Derived from Silk for Ultrahigh-Capacity Battery Anodes and Supercapacitors

Jianhua Hou, Chuanbao Cao,* Faryal Idrees, and Xilan Ma

Reseach Center of Materials Science, Beijing Institute of Technology, Beijing 100081, People's Republic of China

ABSTRACT Hierarchical porous nitrogen-doped carbon (HPNC) nanosheets (NS) have been prepared *via* simultaneous activation and graphitization of biomass-derived natural silk. The as-obtained HPNC-NS show favorable features for electrochemical energy storage such as high specific surface area (S_{BET}: 2494 m^2/g), high volume of hierarchical pores (2.28 cm^3/g), nanosheet structures, rich N-doping (4.7%), and defects. With respect to the multiple synergistic effects of these features, a lithium-ion battery anode and a two-electrode-based supercapacitor have been prepared. A reversible lithium storage capacity of 1865 mA h/g has been reported, which is the highest for N-doped carbon anode materials to the best of our knowledge. The HPNC-NS supercapacitor's electrode in ionic liquid electrolytes exhibit a capacitance of 242 F/g and energy density of 102 W h/kg (48 W h/L), with high cycling life stability (9% loss after 10 000 cycles). Thus, a high-performance Li-ion battery and supercapacitors were successfully assembled for the same electrode material, which was obtained through a one-step and facile large-scale synthesis route. It is promising for next-generation hybrid energy storage and renewable delivery devices.

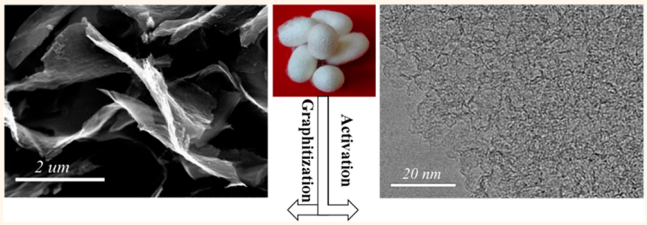

KEYWORDS: Li-ion battery · supercapacitors · hierarchical porous · nitrogen-doped · carbon nanosheets

Fabricating devices for high-performance energy storage has great importance for the advancement of electrical vehicles and renewable energy.[1,2] Currently, carbon is recognized as the leading electrode material for anodes of commercial lithium-ion batteries (LIBs) and electrochemical supercapacitors due to its low cost, high electrical conductivity, good chemical stability, environmental friendliness, and long cycling life.[1−11] Unfortunately, most common graphitic carbons have relatively low theoretical capacity (372 mA h/g) and poor rate performance and do not meet the requirement of high-energy and -power LIBs.[12−14] As for electrical double-layer capacitors (EDLCs), commercially available activated carbons (ACs) offer limited control over specific surface area, conductivity, pore size distribution (PSD), and porosity, suffering from the limitations of commercial supercapacitors (5 Wh/kg).[1] Therefore, there is a critical need to develop new and advanced carbon-based materials with enhanced characteristics (hierarchical pores, 2D-nanostructures, high specific surface area (S_{BET}), heteroatom modification, high electrical conductivity, *etc.*) through a facile synthesis route for highly efficient energy storage devices.

Over the years, many new carbonaceous materials have been developed to address various inherent problems: (i) high S_{BET} for active sites facilitates charge capacity;[15−17] (ii) designing novel nanostructures can shorten the diffusion pathways and offer minimized diffusive resistance to mass transport on a large electrode/electrolyte interface;[18−26] (iii) hierarchical porosity (intertwined micro-, meso-, and macropores) can offer rapid ion transport with improved rate capability;[17,21−23] (iv) introducing defects and heteroatom and/or functional groups can increase available active sites and effectively modulate their electronic and chemical character.[22,24,27−30] It is without doubt that the multiple synergistic effects of the above-mentioned features will boost the related performance of carbonaceous materials in energy storage

* Address correspondence to cbcao@bit.edu.cn.

Received for review October 8, 2014 and accepted February 21, 2015.

Published online February 22, 2015
10.1021/nn506394r

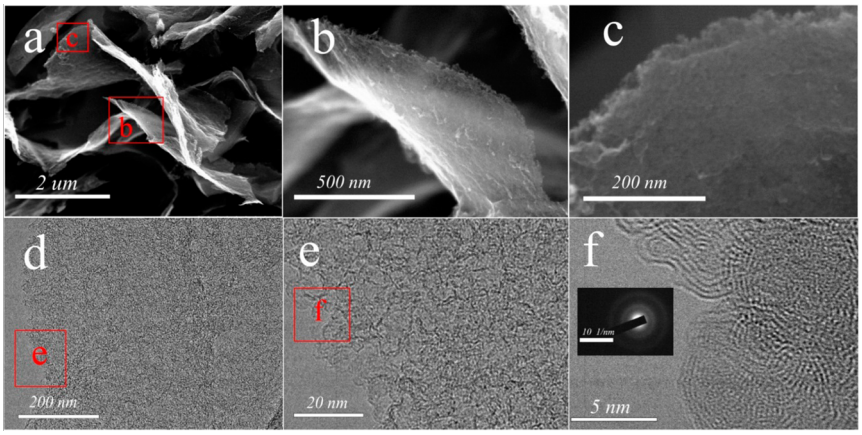

Figure 1. SEM images (a−c) and TEM (d−f) of an HPNC-NS.

applications. Unfortunately, there are still huge challenges in satisfying all the aforementioned characteristics of carbonaceous materials simultaneously through existing technologies. In addition, from a long-term perspective, looking for biorenewable carbon sources along with developing their simple and easy synthesis routes is essential and highly needed.[31]

On the basis of these concerns, the metal salts $FeCl_3$ and $ZnCl_2$ not only facilitate dissolution of natural silk to reformulate it into new materials (regenerated silk fibroin)[32] but also act as effective activation−graphitization agents that can introduce a porous structure with plentiful micro- and mesopores for a high surface area. In the dissolution process, the silk fibroin lamellar-like layered structure is formed by self-assembly of hydrophilic and hydrophobic blocks in an aqueous system.[20] Like cyclization, a lamellar-like layered structure can easily be converted to carbon materials undergoing structural transformation.[33,34] Therefore, novel carbon-based nitrogen-doped hierarchical porous nanosheets (HPNC-NSs) can be prepared from a lamella-like multiple layer structure *via* the metal salt activation−graphitization process. The as-obtained unique graphitized HPNC-NS possesses remarkable features of high S_{BET} (2494 m^2/g) with abundant active site dispersion over hierarchical pores (2.28 m^3/g) to facilitate rapid charge transfer, high charge capacity, easy electrolyte access, adequate mass transport, and minimized polarization effects.[15−22] Moreover, rich heteroatom doping (*e.g.*, N: 4.7%) and defects in HPNC-NSs enhance the electrochemical reactivity and electronic conductivity,[22,24,27−30] which contributes to the exceptional performance as well. These characteristics have favorable multiple synergistic effects, beneficial for LIB and supercapacitor applications, which require high energy and power density.

RESULTS AND DISCUSSION

As seen from SEM in Figure 1a−c, the architecture of an HPNC-NSs with 2D nanosheet morphology and the thickness of the nanosheets can be estimated in the range of 15 to 30 nm, which is consistent with AFM analysis (Figure S1). The folds of the nanosheets effectively limit them from stacking together. A continuous 2D porous network is observed (Figure 1c−e). Furthermore, the TEM images show progressively more graphene ordering going from Figure 1e to Figure 1f. In addition, the HRTEM image (Figure 1f) shows that the thickness of the graphene sheets is around 2 nm with 4 to 5 layers of graphene. The layer-to-layer distance is 0.40 nm, which is confirmed by the (002) XRD peaks. The nanosheet architecture not only offers minimum diffusive resistance to mass transport on a large electrode/electrolytes interface for charge-transfer reaction but also provides easy ion transport by shortening the diffusion pathways.[18−25] The nanopores can serve as active sites for ions, while conductive graphene layers function as paths for fast electron transfer and intercalation sites for ions.[15−22] All of these are important in delivering excellent capacitance and high rate performance of electrodes.

The X-ray diffraction (XRD) pattern of HPNC-NSs can be seen in Figure 2a. Two characteristic peaks of the sample are located at around $2\theta = 26°$ corresponding to the (002) and 44° corresponding to the (101) plane. These diffraction planes belong to the hexagonal graphite (JCPDS card no. 41-1487).[36] The Raman spectrum of HPNC-NS (Figure 2b) presents a G-band at 1593 cm^{-1} (related to graphitic carbon) and a D-band at 1357 cm^{-1} (associated with defects). Further I_G/I_D = 1.15 by Raman results, the relatively highly graphitized HPNC-NS,[22,37] offering good electric conductivity, which is consistent with the XRD. Elemental analysis shows C, N, H, and O contents in HPNC-NS are 89.1, 4.7, 1.4, and 4.4 wt %, respectively, which is consistent with the EDX (Table S1 and Figure S2). XPS measurements are performed in order to probe further for the chemical identification of the heteroatoms in the functionalized HPNC-NS. These results agree with the elemental analysis; that is, C 1s, N 1s, and O 1s peaks can be seen in the XPS spectra (Figure S3). The high-resolution N 1s spectra (Figure 2b) can be fitted by two peaks

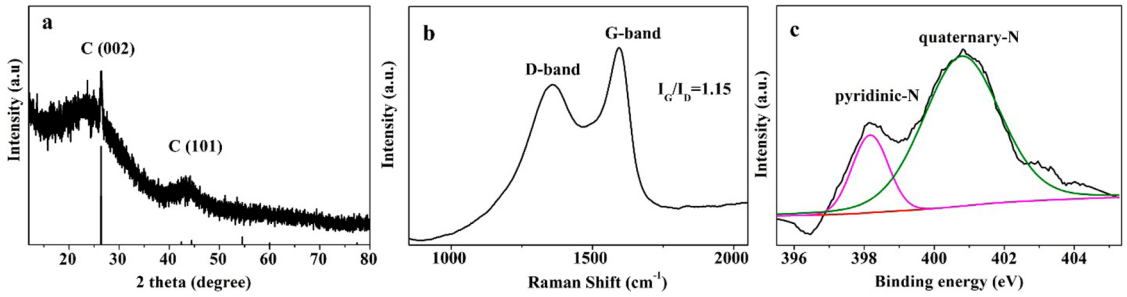

Figure 2. (a) XRD patterns, (b) Raman spectrum, and (c) high-resolution spectrum of the N 1s XPS peak of the HPNC-NS.

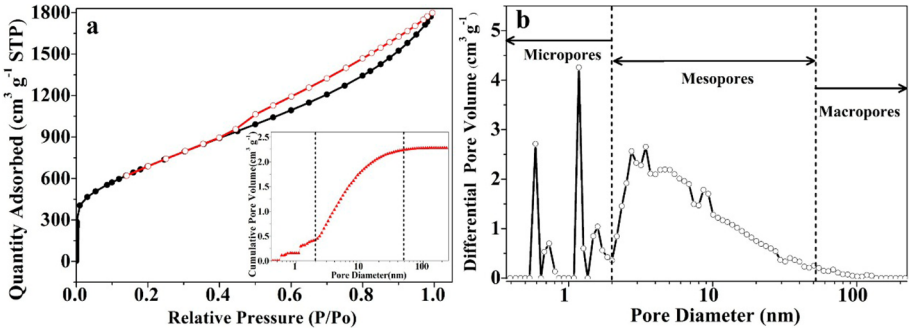

Figure 3. Nitrogen adsorption−desorption isotherm (inset: cumulative pore volume) (a) and pore size distribution (b) of an HPNC-NS.

located at 400.9 due to a quaternary (N-Q) group and at 398.2 eV attributed to a pyridinic nitrogen group (N-6).[27] This exhibits the partial conversion of N atoms within the amino group of silk into N-6 or N-Q during the carbonization process. The high-resolution C 1s spectrum demonstrates the presence of a C−N bond (285.3 eV) (Figure S3). The abundance of N-Q (73%) in HPNC-NS is much more compared to N-6 (27%). This indicates N atoms mainly reside in graphene layers instead of at the periphery. As indicated by a previous study's results,[38] the N atom substituents (N-Q) within the graphene layers could enhance the electronic conductivity of carbon materials, which is highly needed for electrodes with high conductivity.[24] Furthermore, for pseudocapacitive interactions initial active sites can be facilitated by easily reachable N-Q and N-6 groups.[39,40] In addition, the presence of N atoms produces defects in carbon as well as creates additional active sites for Li^+ storage.[22,24,27−30]

To further determine the porosity of HPNC-NS, N_2 adsorption−desorption isothermal analysis is executed. For strong N_2 adsorption HPNC-NS showed an I/IV-type adsorption−desorption isothermal curve. The behavior is observed at low pressure with slight sheer adsorption within the 0.7−1.0 relative pressure range (Figure 3a). It is much different from the I-type associated with traditional activated carbon adsorption−desorption isotherms.[15,20,41] The collective curves of HPNC-NS indicate that micro-, meso-, and/or macropores exist in HPNC-NS. The specific surface area is found to be 2494 m^2/g, as calculated by the Brunauer−Emmett−Teller (BET) method. This high specific surface area can offer an ample electrode/electrolyte interface for ion or charge accumulation. The HPNC-NS pore size distribution is calculated using the conventional DFT method on the N_2 adsorption isotherm part as shown in Figure 3b. The micropores are centered at 0.59 and 1.29 nm. A continuous pore distribution within the range of 2−100 nm is found, which is almost in a linear decline relation with pore size. The total pore volume of HPNC-NS is found to be 2.23 cm^3/g, the micropore volume 0.41 cm^3/g, the macro-/mesopore volume 1.82 cm^3/g, the micropore/total pore volume ratio 18%, the macro-/mesopores/total pore volume ratio 82%, and the average pore size diameter 4.6 nm. As compared to the conventional activated and microporous carbon synthesized from silk proteins by KOH activation (which typically possesses pores of 4 nm or smaller),[15,20,41,42] the present high volume of macro-/mesopores (1.82 cm^3/g) is more favorable for rapid diffusion of ions and results in an exceptionally enhanced rate performance electrode material. In addition, the appropriate proportion of micropores guarantees their high specific surface area. Such a hierarchical porous nanosheet architecture demonstrated that the synergistic effect of macro-, meso-, and microporosity is extremely beneficial for both high-rate performance and high-density energy storage.[31] The applications of such high specific surface area carbon nanosheets with a variety of pore sizes are extendable to other properties such as high-density hydrogen storage.[43]

As a new type of N-doped carbon-based material of a hierarchical porous nanosheet structure, the HPNC-NS is

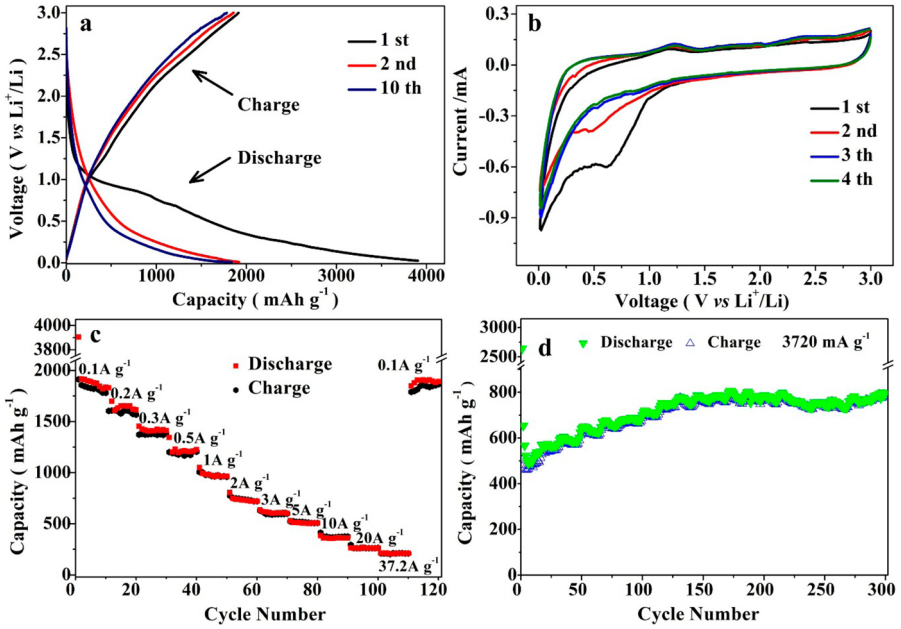

Figure 4. Electrochemical performances of HPNC-NS: (a) charge−discharge curves at 0.1 A/g; (b) CVs of the initial four cycles at a scan rate of 0.1 mv/s; (c) capacity over cycling at different rates; and (d) cyclability at 3720 mA/g.

suitable as a high-performance electrode material for energy storage. For example in LIBs, its hierarchical porous nanosheet structure with high surface area is highly desired because it can cut down the transport length for lithium ions as well as proffer a large electrode/electrolyte interface, which is favorable for charge-transferring reactions.[15] Doping electron-rich N in the partial graphite carbon nanosheet structure with defects that are chemically active[22,24,27−30] can further enhance the electrical conductivity and reactivity by giving more available active sites for Li^+ adsorption[43−45] and improving Li^+ storage ability.[45]

Electrochemical Performance of HPNC-NS as a LIB Anode. The electrochemical performance of an HPNC-NS as a LIB anode is presented in Figure 4. Figure 4a shows the charging/discharging behavior profiles of HPNC-NS for the first, second, and tenth cycles at a current density of 0.1 A/g with a voltage range of 0.01−3.0 V. The initial reversible capacity is 1913 mA h/g, 5 times more as compared to the theoretical capacity of graphite (372 mA h/g), indicating that there are some different mechanisms for lithium storage in this graphite.[12,46] The initial Coulombic efficiency of HPNC-NS is 49.2% at 0.1 A/g, which is higher than that of 2D mesoporous carbon nanosheets (~21%).[18,19] Moreover, a large irreversible capacity of 1991 mA h/g is measured in the first cycle, which can endorse formation of a solid electrolyte interphase (SEI) layer on the relatively large specific surface area of the HPNC-NS (2494 m^2/g)[15,16] and trap lithium ions in this SEI film and/or from irreversible lithium insertion into special positions in the vicinity of residual H atoms in the carbon material.[47] The continuous trapped Li ions may fracture and re-form a thick SEI film during the initial capacity fading period.[48] Furthermore, after the first cycle the capacity becomes stable and reversible. The Coulombic efficiencies of the HPNC-NS at low and high current density remain more than ~95% after the first few cycles.

In the first discharge, the apparent area centered at 0.62 V was also observed, which radically drops in the second cycle. This behavior is associated with irreversible reactions leading to an SEI layer.[15,16] The cyclic voltammetry (CV) curves were quite similar after the third cycle, which indicates a stable state of the HPNC-NS is attained. The capacity above 0.5 V is attributed to manifold defects of 2D architectures and layers, pores, and cavities among these, boundaries between differently oriented graphite crystallites, and Li binding with heteroatoms, while that below 0.5 V is associated with lithium metal under potential deposition.[49−51] In addition, the more active sites for Li storage were provided by increasing the number of defects and vacancies by incorporation of a nitrogen element in the carbon nanosheet framework.[43−45] During the Li-extraction process, an appreciable potential hysteresis can be observed, showing that the inserted lithium ions were removed in a wide voltage range of 0.01−3 V. Peaks at 0.1 and 1.14 V were observed, which are associated with Li extraction from graphene layers and pore structures/defects, respectively.[13,22,45] A relatively weak peak was observed between 2 and 3 V, which arose due to Li binding with heteroatoms on the surface of the anode materials.[13,45] Furthermore, Li ion adsorption and insertion/extraction on surfaces/defects of HPNC-NS was noticed, which may be ascribed to the high S_{BET} with copious micro- and mesopores and reversible binding at heteroatoms[17,24,52−55]

(experimental details provided in the Supporting Information Figures S5 and S6). Therefore, multiple Li storage positions in HPNC-NS electrodes might explain why the carbon has a much higher capacity.

With the increase of charge−discharge current densities from 0.2 to 37.2 A/g, the reversible capacities are *ca.* 1604, 1372, 1201, 1005, 776, 629, 523, 373, and 261 mA h/g at 0.2, 0.3, 0.5, 1, 2, 3, 5, 10, and 20 A/g, respectively (Figure 4c). Even at an ultrahigh current density of 37.2 A/g (100 C), a large reversible capacity of 212 mA h/g is obtained. After cycling at various rates when the current density is again 0.1 A/g, the specific capacity can still be recovered to 1865 mA h/g, implying highly stable cycling performance and good reversibility. To the best of our knowledge, the present specific capacity (1865 mA h/g) is 5 times greater as compared to the theoretical capacity of graphite (372 mA h/g) and is the highest capacity that has been reported so far for N-doped carbon anode materials.

As shown in Figure 4d and Figure S7, the HPNC-NS anode exhibits high cyclability and capacity, while the reversible battery capacity is 1287 and 512 mA h/g in the first cycle, which steadily increases to 1401 and 714 mA h/g after 300 cycles at 372 and 3720 mA/g, respectively. After a large initial loss of capacity, the hierarchical porous nanosheet structure is efficiently reactivated and the unique nanostructure of HPNC-NS effectively shortens the diffusion length, providing fast mass transport and minimized polarization effects. The self-optimized thin and stable SEI layer shows long-term cycling, significantly enhancing the lithium storage performance at high rates.[48,56,57] Moreover, the ac impedance spectroscopy (EIS) results in Figure S8, the initial EIS and after 300 cycles help to further understand the advantages of HPNC-NS structure for excellent electrochemical performance. The EIS spectrum (Figure S8) after 300 cycles presented a depressed semicircle and a smaller interfacial charge-transfer resistance, indicating good electronic conductivity of the material and high Li^+ ion transfer speed across interfaces between the electrolyte and active electrode materials.[22,47] The high reversibility and good rate capability of HPNC-NS are superior or comparable to many other carbon-based materials (Figure 4c and d), including 2D mesoporous carbon nanosheets (C), N-doped carbon materials (N−C), N,S-co-doped carbon materials (N,S−C), metal oxide and N-doped carbon composites (MOx/N−C), metal and N-doped carbon composites (M/N−C), and metal sulfide and carbon composites (MS_x/C) as summarized in Table S2. Examples can be found for mesoporous graphene nanosheets (770 mAh/g at 0.1 A/g),[18] N-doped carbon nanofibers (637 mA h/g at 2 A/g),[15] N,S-co-doped porous graphene (860 mA h/g at 0.5 A/g),[35] B-doped carbon nanosheets/Fe_2O_3 (980 mA h/g at 0.1 A/g),[58] SnO_2@N-doped graphene sheets (1074 mA h/g at 0.5 A/g),[59] Sn/N−C (560 mA h/g at 2A/g),[60] and MoS_x/CNTs (1126 mA h/g at 0.05 A/g).[61]

To increase the energy density of electrical double layer capacitors, one can enlarge the interfacial area between the electrodes and electrolyte through introducing nanopores and by using wider voltage range electrolytes such as ionic liquids (ILs).[26] However, commercially available ACs have poor S_{BET} (<2000 m^2/g), and the very smal pore size, less than 0.6 nm,[62] limits the access of IL electrolyte ions.[63] The relatively large ion sizes and high viscosity of ionic liquids needs 2D-hierarchical porous nanostructures, which offer minimized diffusive resistance for mass transport by macropores and effective S_{BET}.[21,32] The presence of nitrogen also enhances the capacitance by providing a high pseudocapacitance *via* pseudocapacitive redox reactions and improved polar properties. Also it improves the electrical conductivity and wettability, which further enhances the ion-transfer efficiency.[20,40,41]

Electrochemical Behavior of HPNC-NS for Supercapacitors. The high S_{BET} and hierarchical porous architectures of HPNC-NS are very important for electrochemical supercapacitors as well in the $EMIMBF_4$ electrolyte. Figure 5a shows that the CV curves from 0 to 3.5 V demonstrated obvious Faradaic humps at low scan rates, which suggest that the capacitive response is due to the combined effect of redox reactions and electrical double-layer formation. In addition,the samples maintain a roughly rectangular shape even at high scan rates. This can be ascribed to the enlarged size of pores in the HPNC-NS, which indicate a fast and efficient charge transfser rate. HPNC-NSs display symmetric charge−discharge curves (Figure 5b), exhibiting only a very small *IR* drop at a high current density. At a current density of 0.1 A/g, the high specific capacitance (for a single electrode) of 242 F/g (113 F/cm^3) was obtained for HPNC-NS (Figure 5c). The value is much higher than that of commercial ACs (<100 F/g, <60 μF/cm^3).[1−3] Moreover, the synthesized products still retain high values of 213 F/g (100 F/cm^3 and ~88% capacitance retention) and 155 F/g (73 F/cm^3 and ~64% capacitance retention) at a high current density of 1 and 10 A/g, respectively. The high-rate supercapacitor results are due to simultaneously synergistic effects; that is, the nanosheet's architecture has shortened the transport length of ions, hierarchical porous structure has enhanced the liquid electrolyte transport between the electrode and ions, and the high S_{BET} of the active site provided a smooth and convenient electron/ion-transport path. Moreover, the relatively highly graphitized structure of the HPNC-NS with N-doping offers good electrochemical reactivity and electric conductivity, favorably contributing to the exceptional performance.[20,40,41]

Therefore, the capacitances obtained in this work are higher than carbon obtained from silk protein by

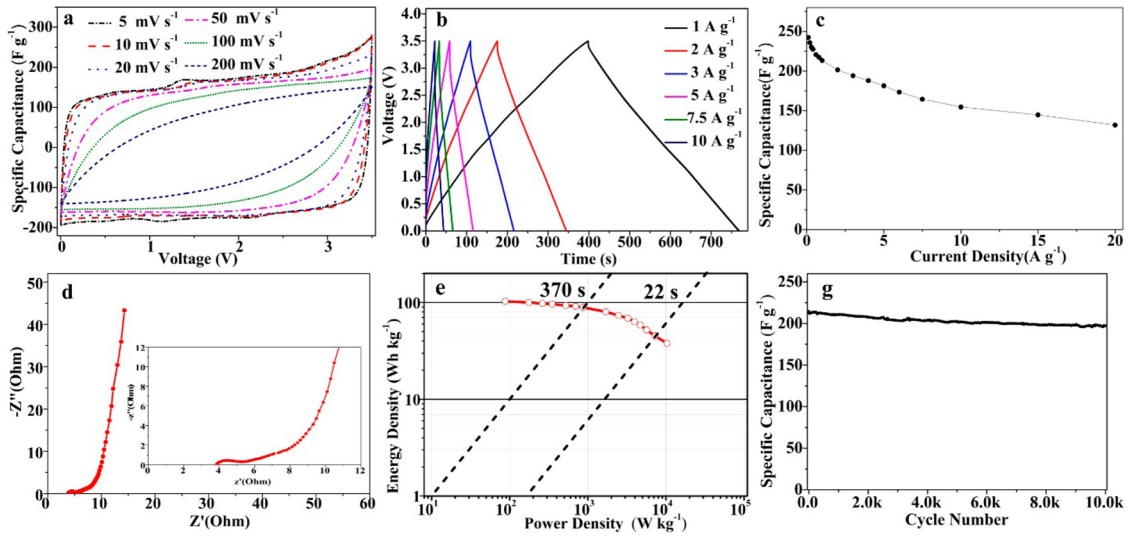

Figure 5. Electrochemical performance of HPCN-NS for a two-electrode system using $EMIMBF_4$ as IL electrolytes at room temperature. (a) CV curves for various scan rates; (b) galvanostatic charge/discharge curves for various current densities; (c) specific capacitance as a function of current densities; (d) Nyquist plots; (e) Ragone plot of symmetrical supercapacitors; (g) cycling stability at a current density of 2A/g up to 10 000 cycles.

KOH activation[20] (168 F/g at 0.8 A/g), human hair,[64] leaves[65] (107 F/g, 88 F/g at 2 A/g), hemp,[66] potassium citrate[67] (134 F/g, 54 F/cm^3 at 5 A/g), and rice bran (133 F/g at 10 A/g)[68] and even greater than some novel carbon materials such as carbon nanotube arrays[69] (120−170 F/g at 1A/g) and a-MEGO[70] (activated microwave-expanded graphite oxide, 50 F/cm^3 for 0.3 g/cm^3), and more surprisingly these are comparable or superior to high density graphene-based electrodes achieved through a compressed a-MEGO (110 F/cm^3 for 0.75 g/cm^3)[71] and partially reduced GO paper (95 F/cm^{-3} for 0.46 g/cm^3).[72] From the EIS results in Figure 5d, HPNC-NSs not only have a relatively low equivalent series resistance but also have shown a much shorter Warburg region. A Ragone plot for symmetrical HPNC-NS supercapacitors depicts that the specific energy density is about 90.0 Wh/kg (42.3 Wh/L) at power densities of 875 W/kg (∼370 s), while the energy density remains as high as 52.5 Wh/kg (24.7 Wh/L) at power densities of 8750 W/kg (∼22 s), which is comparable to commercial devices (pseudocapacitors <30 Wh/kg),[1−3] a hybrid supercapacitor (48−60 Wh/kg),[73−75] and those achieved with advanced activated carbons.[69−72] In our case the carbon weight is ∼25% of the total mass of a packaged commercial EC,[76] *i.e.*, a specific energy of 22.5 and 15.1 Wh/kg (10.6 and 6.2 W/L), which is expected for a real packaged device and 4 times higher than commercial ACs-based supercapacitors (5 Wh/kg). The HPNC-NS also showed a high stability of ∼92% after 10 000 cycles at a current density of 2 A/g compared with the initial materials (Figure 5g), which is due to the corrosive presence of the functional groups.[77]

The above results indicate HPNC-NS as a promising material for advanced electrodes for both LIBs and electrochemical supercapacitors. The HPNC-NS's high S_{BET}, unique hierarchical porous nanosheet structures, and partially graphitized and heteroatom-modified carbon leads to extraordinarily large and stable energy storage performance. Other than these, their favorable multiple synergistic effects are the following:

(i) The superhigh S_{BET} (2494 m^2/g) for active site dispersion over meso-/micropores provides an appropriate electrode/electrolyte interface to facilitate fast charge transfer and charge capacity, absorb (Li^+) ions, and minimize polarization effects.[15−17]

(ii) The thin nanosheets can shorten the transport length of ions, while the high volume of macro-/mesopores (1.82 cm^3/g) on their surface can supply favorable accessibility, adequate mass transport, and facile transport channels for ions.[17,21−23]

(iii) The performance can be enhanced to an exceptional level by N-doping (4.7%) in HPNC-NSs with relatively highly graphitized carbon walls. This results due to possible enhancement of electrochemical reactivity, defects sites, and electronic conductivity.[22,24,27−30]

(iv) The above three elements have favorable multiple synergistic effects: interaction and easy transportation to improve the HPNC-NS electrode material performance for superior energy storage applications.

CONCLUSION

In summary, the novel nanostructured HPNC-NS has been prepared *via* simultaneous activation and graphitization and a facile large-scale synthesis route. The as-obtained HPNC-NS consisted of 2D nanosheet-architecture carbon with high hierarchical porosity (2.28 m^3/g), high surface area (2494 m^2/g), rich N-doping

(4.7%), and defects. These characteristics have favorable multiple synergistic effects, beneficial for high-performance energy storage-related applications. We obtained the highest reported reversible lithium storage capacity (1865 mAh/g) for any N-doped carbon anode materials. Tested as a supercapacitor in an ionic liquid electrolyte two-electrode system, the carbons exhibited a capacitance of 242 F/g, energy density of 102 Wh/kg, with high cycling life stability (9% loss after 10 000 cycles). Our results indicate that the HPNC-NC is promising for next-generation hybrid energy storage and renewable delivery devices with high power and energy density. Moreover, the obtained HPNC-NS can also be used for a sodium ion battery, an adsorbent, a catalyst, and hydrogen storage.

EXPERIMENTAL SECTION

Materials. Silk was obtained from Anhui, China. Ferric chloride hexahydrate ($FeCl_3 \cdot 6H_2O$), zinc chloride ($ZnCl_2$), and hydrochloric acid (HCl) used were of analytical grade. 1-Ethyl-3-methylimidazolium tetrafluoroborate ($EMIMBF_4$ > 99%, water content <100 ppm) was purchased from the Linzhou Branch of Materials Science and Technology Co.

Synthesis of Hierarchical Porous Nitrogen-Doped Carbon (HPNC-NS). Six grams of natural silk without any further treatment was mixed with 15 g of $ZnCl_2$ in a 2.5 M (100 mL) $FeCl_3$ solution as an initial step. The solution was continuously stirred and evaporated at 60 °C for 4 h. Carbon precursor was obtained by further drying at 80 °C in a conventional oven. Activation and graphitization were followed by annealing carbon up to 900 °C for 1 h under a N_2 atmosphere in a tubular furnace with ramp rate of 2 °C/min. The resulting dark solid was ground to bulk, washed with a 1 M HCl solution to remove iron species, and then washed with deionized water. It was dried at 120 °C for 12 h, and HPNC-NS was obtained as a final product.

Electrochemical Testing. The electrochemical performance of the HPNC-NS was measured in ionic liquid electrolytes for a two-electrode system. A 85 wt % amount of obtained carbon, 10 wt % of acetylene black, and 5 wt % of PTFE binder were used for the electrode preperation. The mixture was pasted on aluminum foil of 11 mm in diameter and then dried under vacuum at 120 °C for 6 h. After drying, the electrodes were pressed under 10 MPa for 30 s. A 6−8 mg amount was loaded on an area of 1 cm^2. As a separator, a cellulose film (TF4840, NKK) was used. The calculated densities of the electrode material are provided in Supporting Information Figure S3. Cyclic voltammetry, galvanostatic charge/discharge, and EIS tests were measured using a CHI660D electrochemical workstation. Impedance spectra were measured for a 0.01 Hz to 10 kHz frequency range with a ±5 mV voltage amplitude. The cutoff charge voltage was set at 0 to 3.5 V for the $EMIMBF_4$ electrolyte. Specific capacitance for a single electrode was calculated by using eq 1:

$$c_g = \frac{2I}{(dV/dt)m} \quad (1)$$

where I (A) = discharge current, dV/dt (V s^{-1}) = slope measured through the discharge curve after ohmic drop, and m (g) = active material mass for a single electrode. The specific energy density (E_{cell}) and specific power density (P_{cell}) for symmetrical supercapacitors were also calculated by using eqs 2 and 3:

$$E_{cell} = \frac{c_g \Delta V}{8 \times 3.6} \quad (2)$$

$$P_{cell} = \frac{E_{cell}}{t} \quad (3)$$

where ΔV (V) = cell voltage after ohmic drop and t (h) = discharge time.

For the battery test, copper foil of 14 mm in diameter was used as current collector. A 80 wt % amount of obtained carbon, 10 wt % of acetylene black, and 10 wt % of PVDF binder were used for the electrode preparation. Around 1.5 mg of active material was pasted on a single electrode. The battery was assembled in an argon-filled glovebox (with O_2 < 1 ppm, H_2O < 1 ppm) by using 2032 coin-type cells, polyethene as the separator, Li metal foil as the counter electrode, and 1 M $LiPF_6$ (solution with ethylene carbonate−dimethyl carbonate) as the electrolyte.

Chemical Analysis and Textural Characterization. In order to see the morphology more clearly, field emission scanning electron microscopy (FSEM) and transmission electron microscopy (TEM) tests were performed using a Hitachi S-4800 and JEOL-2100, respectively. The powder X-ray diffraction pattern from 10° to 80° was measured using a PANalytical-X-pert diffractometer (Cu Kα radiation at 40 kV and 40 mA). The Raman spectrum was measured at 514 nm excitation by a Renishaw apparatus. A Thermo Fisher Scientific (EA-1108-CHNS-O) elemental analyzer was used to measure elemental ratios. An Axis Ultra spectrometer was used for XPS analysis. The nitrogen adsorption−desorption isotherm was measured at 77 K and a relative pressure p/p_0 of 3.3×10^{-7}−0.995 by using a Micromeritics-ASAP-2020. BET and density functional theory (DFT) tests were performed to measure the specific surface area and pore size distribution.

Conflict of Interest: The authors declare no competing financial interest.

Acknowledgment. C-B.C. designed the experiments. J-H.H. prepared the samples and performed the experiments. F.I. and X-L.M. participated in interpreting and analyzing the data. C-B.C. and J-H.H. wrote the manuscript. This work was supported by the National Natural Science Foundation (NNSF), China (grant no. 50972017).

Supporting Information Available: Additional experimental details and further analysis results. This material is available free of charge *via* the Internet at http://pubs.acs.org.

REFERENCES AND NOTES

1. Simon, P.; Gogotsi, Y. Materials for Electrochemical Capacitors. *Nat. Mater.* **2008**, *7*, 845–854.
2. Parlett, C. M.; Wilson, K.; Lee, A. F. Hierarchical Porous Materials: Catalytic Applications. *Chem. Soc. Rev.* **2013**, *42*, 3876–3893.
3. Zhai, Y. P.; Dou, Y. Q.; Zhao, D. Y.; Fulvio, P. F.; Mayes, R. T.; Dai, S. Carbon Materials for Chemical Capacitive Energy Storage. *Adv. Mater.* **2011**, *23*, 4828–4850.
4. Miller, J. R.; Simon, P. Electrochemical Capacitors for Energy Management. *Science* **2008**, *321*, 651–652.
5. Evanoff, K.; Khan, J.; Balandin, A. A.; Magasinski, A.; Ready, W. J.; Fuller, T. F.; Yushin, G. Towards Ultrathick Battery Electrodes: Aligned Carbon Nanotube-Enabled Architecture. *Adv. Mater.* **2012**, *24*, 533–537.
6. Li, Y.; Fu, Z. Y.; Su, B.-L. Hierarchically Structured Porous Materials for Energy Conversion and Storage. *Adv. Funct. Mater.* **2012**, *22*, 4634–4667.
7. Yang, X.; Cheng, C.; Wang, Y.; Qiu, L.; Li, D. Liquid-Mediated Dense Integration of Graphene Materials for Compact Capacitive Energy Storage. *Science* **2013**, *341*, 534–537.
8. Zhang, L. L.; Zhao, X. S. Carbon-Based Materials as Supercapacitor Electrodes. *Chem. Soc. Rev.* **2009**, *38*, 2520–2531.
9. Marco-Lozar, J. P.; Kunowsky, M.; Suárez-García, F.; Carruthers, J. D.; Linares-Solano, A. Activated Carbon Monoliths for Gas Storage at Room Temperature. *Energy Environ. Sci.* **2012**, *5*, 9833–9842.

10. Jiang, J.; Zhu, J.; Ai, W.; Fan, Z.; Shen, X.; Zou, C.; Liu, J.; Zhang, H.; Yu, T. Evolution of Disposable Bamboo Chopsticks into Uniform Carbon Fibers: A Smart Strategy to Fabricate Sustainable Anodes for Li-Ion Batteries. *Energy Environ. Sci.* **2014**, *7*, 2670–2679.
11. Béguin, F.; Presser, V.; Balducci, A.; Frackowiak, E. Carbons and Electrolytes for Advanced Supercapacitors. *Adv. Mater.* **2014**, *26*, 2219–2251.
12. Kaskhedikar, N. A.; Maier, J. Lithium Storage in Carbon Nanostructures. *Adv. Mater.* **2009**, *21*, 2664–2680.
13. Guo, B.; Wang, X.; Fulvio, P. F.; Chi, M.; Mahurin, S. M.; Sun, X.-G.; Dai, S. Soft-Templated Mesoporous Carbon-Carbon Nanotube Composites for High Performance Lithium-Ion Batteries. *Adv. Mater.* **2011**, *23*, 4661–4666.
14. Mukherjee, R.; Thomas, A. V.; Datta, D.; Singh, E.; Li, J.; Eksik, O.; Shenoy, V. B.; Koratkar, N. Defect-Induced Plating of Lithium Metal within Porous Graphene Networks. *Nat. Commun.* **2014**, *5*, 3710–3719.
15. Qie, L.; Chen, W.-M.; Wang, Z.-H.; Shao, Q.-G.; Li, X.; Yuan, L.-X.; Hu, X.-L.; Zhang, W.-X.; Huang, Y.-H. Nitrogen-Doped Porous Carbon Nanofiber Webs as Anodes for Lithium Ion Batteries with a Superhigh Capacity and Rate Capability. *Adv. Mater.* **2012**, *24*, 2047–2050.
16. Chen, Y.; Li, X.; Park, K.; Song, J.; Hong, J.; Zhou, L.; Mai, Y. W.; Huang, H.; Goodenough, J. B. Hollow Carbon-Nanotube/Carbon-Nanofiber Hybrid Anodes for Li-Ion Batteries. *J. Am. Chem. Soc.* **2013**, *135*, 16280–16283.
17. Qie, L.; Chen, W.; Xu, H.; Xiong, X.; Jiang, Y.; Zou, F.; Hu, X.; Xin, Y.; Zhang, Z.; Huang, Y. Synthesis of Functionalized 3D Hierarchical Porous Carbon for High-Performance Supercapacitors. *Energy Environ. Sci.* **2013**, *6*, 2497–2504.
18. Fang, Y. Y.; Lv, Y.; Che, R. C.; Wu, H. Y.; Zhang, X. H.; Gu, D.; Zheng, G. F.; Zhao, D. Y. Two-Dimensional Mesoporous Carbon Nanosheets and Their Derived Graphene Nanosheets: Synthesis and Efficient Lithium Ion Storage. *J. Am. Chem. Soc.* **2013**, *135*, 1524–1530.
19. Li, J.; Yao, R.; Bai, J.; Cao, C. Two-Dimensional Mesoporous Carbon Nanosheets as a High-Performance Anode Material for Lithium-Ion Batteries. *ChemPlusChem* **2013**, *78*, 797–800.
20. Yun, Y. S.; Cho, S. Y.; Shim, J.; Kim, B. H.; Chang, S.-J.; Baek, S. J.; Huh, Y. S.; Tak, Y.; Park, Y. W.; Park, S.; Jin, H.-J. Microporous Carbon Nanoplates from Regenerated Silk Proteins for Supercapacitors. *Adv. Mater.* **2013**, *25*, 1993–1998.
21. Li, Y.; Li, Z.; Shen, P. K. Simultaneous Formation of Ultrahigh Surface Area and Three-Dimensional Hierarchical Porous Graphene-Like Networks for Fast and Highly Stable Supercapacitors. *Adv. Mater.* **2013**, *17*, 2474–2480.
22. Hu, C.; Wang, L.; Zhao, Y.; Ye, M.; Chen, Q.; Feng, Z.; Qu, L. Designing Nitrogen-Enriched Echinus-like Carbon Capsules for Highly Efficient Oxygen Reduction Reaction and Lithium Ion Storage. *Nanoscale* **2014**, *6*, 8002–8009.
23. Liang, Y.; Wu, D.; Fu, R. Carbon Microfibers with Hierarchical Porous Structure from Electrospun Fiber-Like Natural Biopolymer. *Sci. Rep.* **2013**, *3*, 1119–1123.
24. Li, Z.; Xu, Z.; Tan, X.; Wang, H.; Holt, C. M. B.; Stephenson, T.; Olsen, B. C.; Mitlin, D. Mesoporous Nitrogen-Rich Carbons Derived from Protein for Ultra-High Capacity Battery Anodes and Supercapacitors. *Energy Environ. Sci.* **2013**, *6*, 871–878.
25. Chen, Y. M.; Lu, Z. G.; Zhou, L. M.; Mai, Y. W.; Huang, H. T. Triple-Coaxial Electrospun Amorphous Carbon Nanotubes with Hollow Graphitic Carbon Nanospheres for High-Performance Li Ion Batteries. *Energy Environ. Sci.* **2012**, *5*, 7898–7902.
26. Vu, A.; Li, X.; Phillips, J.; Han, A.; Smyrl, W. H.; Buhlmann, P.; Stein, A. Three-Dimensionally Ordered Mesoporous (3DOm) Carbon Materials as Electrodes for Electrochemical Double-Layer Capacitors with Ionic Liquid Electrolytes. *Chem. Mater.* **2013**, *25*, 4137–4148.
27. Wu, Z. S.; Ren, W. C.; Xu, L.; Li, F.; Cheng, H. M. Doped Graphene Sheets as Anode Materials with Superhigh Rate and Large Capacity for Lithium Ion Batteries. *ACS Nano* **2011**, *5*, 5463–5471.
28. Shin, W. H.; Jeong, H. M.; Kim, B. G.; Kang, J. K.; Choi, J. W. Nitrogen-Doped Multiwall Carbon Nanotubes for Lithium Storage with Extremely High Capacity. *Nano Lett.* **2012**, *12*, 2283–2288.
29. Yang, L. J.; Jiang, S. J.; Zhao, Y.; Zhu, L.; Chen, S.; Wang, X. Z.; Wu, Q.; Ma, J.; Ma, Y. W.; Hu, Z. Boron-Doped Carbon Nanotubes as Metal-Free Electrocatalysts for the Oxygen Reduction Reaction. *Angew. Chem., Int. Ed.* **2011**, *50*, 7132–7135.
30. Li, Y. G.; Zhou, W.; Wang, H. L.; Xie, L. M.; Liang, Y. Y.; Wei, F.; Idrobo, J. C.; Pennycook, S. J.; Dai, H. J. An Oxygen Reduction Electrocatalyst Based on Carbon Nanotube-Graphene Complexes. *Nat. Nanotechnol.* **2012**, *7*, 394–400.
31. Dutta, S.; Kevin, A. B.; Wu, C. W. Hierarchically Porous Carbon Derived from Polymers and Biomass: Effect of Interconnected Pores on Energy Applications. *Energy Environ. Sci.* **2014**, *7*, 3574–3592.
32. Jin, H. J.; Park, J.; Karageorgiou, V.; Kim, U. J.; Valluzzi, R.; Cebe, P.; Kaplan, D. L. Water-Stable Silk Films with Reduced β-Sheet Content. *Adv. Funct. Mater.* **2005**, *15*, 1241–1247.
33. Jin, H. J.; Kaplan, D. L. Mechanism of Silk Processing in Insects and Spiders. *Nature* **2003**, *424*, 1057–1061.
34. Watt, W.; Johnson, W. Mechanism of Oxidisation of Polyacrylonitrile Fibres. *Nature* **1975**, *257*, 210–212.
35. Wang, Z. L.; Xu, D.; Wang, H. G.; Wu, Z.; Zhang, X. B. *In Situ* Fabrication of Porous Graphene Electrodes for High-Performance Energy Storage. *ACS Nano* **2013**, *7*, 2422–2430.
36. Hwang, S.; Lee, S.; Yu, J. S. Template-Directed Synthesis of Highly Ordered Nanoporous Graphitic Carbon Nitride through Polymerization of Cyanamide. *Appl. Surf. Sci.* **2007**, *253*, 5656–5659.
37. Dresselhaus, M. S.; Dresselhaus, G.; Saito, R.; Jorio, A. Raman Spectroscopy of Carbon Nanotubes. *Phys. Rep.* **2005**, *409*, 47–99.
38. Lim, S. H.; Li, R.; Ji, W.; Lin, J. Effects of Nitrogenation on Single-Walled Carbon Nanotubes within Density Functional Theory. *Phys. Rev. B: Condens. Matter Mater. Phys.* **2007**, *76*, 195406–195421.
39. Ma, C. C.; Shao, X. H.; Cao, D. P. Nitrogen-Doped Graphene Nanosheets as Anode Materials for Lithium Ion Batteries: A First-Principles Study. *J. Mater. Chem.* **2012**, *22*, 8911–8915.
40. Seredych, M.; Hulicova-Jurcakova, D.; Lu, G. Q.; Bandosz, T. J. Surface Functional Groups of Carbons and the Effects of Their Chemical Character, Density and Accessibility to Ions on Electrochemical Performance. *Carbon* **2008**, *46*, 1475–1488.
41. Armandi, M.; Bonelli, B.; Geobaldo, F.; Garrone, E. Nanoporous Carbon Materials Obtained by Sucrose Carbonization in the Presence of KOH. *Microporous Mesoporous Mater.* **2010**, *132*, 414–420.
42. Wang, J.; Kaskel, S. KOH Activation of Carbon-Based Materials for Energy Storage. *J. Mater. Chem.* **2012**, *22*, 23710–23725.
43. Yang, S. J.; Kim, T.; Im, J. H.; Kim, Y. S.; Lee, K.; Jung, H.; Park, C. R. MOF-Derived Hierarchically Porous Carbon with Exceptional Porosity and Hydrogen Storage Capacity. *Chem. Mater.* **2012**, *24*, 464–470.
44. Wu, Z. S.; Ren, W.; Xu, L.; Li, F.; Cheng, H. M. Doped Graphene Sheets as Anode Materials with Superhigh Rate and Large Capacity for Lithium Ion Batteries. *ACS Nano* **2011**, *5*, 5463–5471.
45. Su, F.; Poh, C. K.; Chen, J. S.; Xu, G.; Wang, D.; Li, Q.; Lin, J.; Lou, X. W. Nitrogen-Containing Microporous Carbon Nanospheres with Improved Capacitive Properties. *Energy Environ. Sci.* **2011**, *4*, 717–724.
46. Yang, S.; Feng, X.; Zhi, L.; Cao, Q.; Maier, J.; Müllen, K. Nanographene-Constructed Hollow Carbon Spheres and Their Favorable Electroactivity with Respect to Lithium Storage. *Adv. Mater.* **2010**, *22*, 838–842.
47. Song, H.; Li, N.; Cui, H.; Wang, C. Enhanced Storage Capability and Kinetic Processes by Pores- and Hetero-Atoms-Riched Carbon Nanobubbles for Lithium-Ion and Sodium-Ion Batteries Anodes. *Nano Energy* **2014**, *4*, 81–87.

48. Sun, H.; Xin, G.; Hu, T.; Yu, M.; Shao, D.; Sun, X.; Lian, J. High-Rate Lithiation-Induced Reactivation of Mesoporous Hollow Spheres for Long-Lived Lithium-Ion Batteries. *Nat. Commun.* **2014**, *5*, 4526–4533.
49. Dahn, J. R.; Zheng, T.; Liu, Y.; Xue, J. S. Mechanisms for Lithium Insertion in Carbonaceous Materials. *Science* **1995**, *270*, 590–593.
50. Mukherjee, R.; Thomas, A. V.; Datta, D.; Singh, E.; Li, J.; Eksik, O.; Shenoy, V. B.; Koratkar, N. Defect-Induced Plating of Lithium Metal within Porous Graphene Networks. *Nat. Commun.* **2014**, *5*, 3710–3719.
51. Mukherjee, R.; Thomas, A. V.; Krishnamurthy, A.; Koratkar, N. Photothermally Reduced Graphene as High-Power Anodes for Lithium-Ion Batteries. *ACS Nano* **2014**, *8*, 7115–7129.
52. Xiao, Y.; Sun, P.; Cao, M. Core-Shell Bimetallic Carbide Nanoparticles Confined in a Three-Dimensional N-Doped Carbon Conductive Network for Efficient Lithium Storage. *ACS Nano* **2014**, *8*, 7846–7857.
53. Mukherjee, R.; Thomas, A. V.; Datta, D.; Singh, E.; Li, J. W.; Eksik, O.; Shenoy, V. B.; Koratkar, N. Defect-Induced Plating of Lithium Metal within Porous Graphene Networks. *Nat. Commun.* **2014**, *5*, 3710–3719.
54. Yin, J.; Qi, L.; Wang, H. Sodium Titanate Nanotubes as Negative Electrode Materials for Sodium-Ion Capacitors. *ACS Appl. Mater. Interfaces* **2012**, *4*, 2762–2768.
55. Ding, R.; Qi, L.; Wang, H. An Investigation of Spinel $NiCo_2O_4$ as Anode for Na-Ion Capacitors. *Electrochim. Acta* **2013**, *114*, 726–735.
56. Wu, H.; Chan, G.; Choi, J. W.; Ryu, I.; Yao, Y.; McDowell, M. T.; Lee, S. W.; Jackson, A.; Yang, Y.; Hu, L.; Cui, Y. Stable Cycling of Double-Walled Silicon Nanotube Battery Anodes through Solid-Electrolyte Interphase Control. *Nat. Nanotechnol.* **2012**, *7*, 309–314.
57. Choi, J.; McDonough, J.; Jeong, S.; Yoo, J.; Chan, C.; Cui, Y. Stepwise Nanopore Evolution in One-Dimensional Nanostructures. *Nano Lett.* **2010**, *10*, 1409–1413.
58. Yang, Y.; Zhang, J.; Wu, X.; Fu, Y.; Wu, H.; Guo, S. Composites of Boron-Doped Carbon Nanosheets and Iron Oxide Nanoneedles: Fabrication and Lithium Ion Storage Performance. *J. Mater. Chem. A* **2014**, *24*, 9111–9117.
59. Zhou, X.; Wan, L. J.; Guo, Y. G. Binding SnO_2 Nanocrystals in Nitrogen-Doped Graphene Sheets as Anode Materials for Lithium-Ion Batteries. *Adv. Mater.* **2013**, *25*, 2152–2157.
60. Zhu, Z. Q.; Wang, S. W.; Du, J.; Jin, Q.; Zhang, T. R.; Cheng, F. Y.; Chen, J. Ultrasmall Sn Nanoparticles Embedded in Nitrogen-Doped Porous Carbon as High-Performance Anode for Lithium-Ion Batteries. *Nano Lett.* **2014**, *14*, 153–157.
61. Shi, Y.; Wang, Y.; Wong, J.; Tan, A. Y.; Hsu, C. L.; Li, L. J.; Lu, Y. C.; Yang, H. Y. Self-Assembly of Hierarchical MoS_x/CNT Nanocomposites ($2 < x < 3$): Towards High Performance Anode Materials for Lithium Ion Batteries. *Sci. Rep.* **2013**, *3*, 2169–2176.
62. Inagaki, S.; Oikawa, K.; Kubota, Y. Effect of Carbon Source on the Textural and Electrochemical Properties of Novel Cage-Type Mesoporous Carbon as a Replica of KIT-5 Mesoporous Silica. *Chem. Lett.* **2009**, *38*, 918–919.
63. Largeot, C.; Portet, C.; Chmiola, J.; Taberna, P. L.; Gogotsi, Y.; Simon, P. Relation between the Ion Size and Pore Size for an Electric Double-Layer Capacitor. *J. Am. Chem. Soc.* **2008**, *130*, 2730–2731.
64. Qian, W.; Sun, F.; Xu, Y.; Qiu, L.; Liu, C.; Wang, S.; Yan, F. Human Hair-Derived Carbon Flakes for Electrochemical Supercapacitors. *Energy Environ. Sci.* **2014**, *7*, 379–386.
65. Biswal, M.; Banerjee, A.; Deo, M.; Ogale, S. From Dead Leaves to High Energy Density Supercapacitors. *Energy Environ. Sci.* **2013**, *6*, 1249–1259.
66. Wang, H.; Xu, Z.; Kohandehghan, A.; Li, Z.; Cui, K.; Tan, X.; Stephenson, T. J.; King'ondu, C. K.; Holt, C. M. B.; Olsen, B. C.; Tak, J. K.; Harfield, D.; Anyia, A. O.; Mitlin, D. Interconnected Carbon Nanosheets Derived from Hemp for Ultrafast Supercapacitors with High Energy. *ACS Nano* **2013**, *7*, 5131–5141.
67. Sevilla, M.; Fuertes, A. B. Direct Synthesis of Highly Porous Interconnected Carbon Nanosheets and Their Application as High-Performance Supercapacitors. *ACS Nano* **2014**, *8*, 5069–5078.
68. Hou, J.; Cao, C.; Idrees, F.; Xu, B.; Hao, X.; Lin, W. From Rice Bran to High Energy Density Supercapacitors: A New Route to Control Porous Structure of 3D Carbon. *Sci. Rep.* **2014**, *4*, 7260–7265.
69. Izadi-Najafabadi, A.; Yasuda, S.; Kobashi, K.; Yamada, T.; Futaba, D. N.; Hatori, H.; Yumura, M.; Iijima, S.; Hata, K. Extracting the Full Potential of Single-Walled Carbon Nanotubes as Durable Supercapacitor Electrodes Operable at 4 V with High Power and Energy Density. *Adv. Mater.* **2010**, *22*, E235–E241.
70. Zhu, Y.; Murali, S.; Stoller, M. D.; Ganesh, K. J.; Cai, W.; Ferreira, P. J.; Pirkle, A.; Wallace, R. M.; Cychosz, K. A.; Thommes, M.; Su, D.; Stach, E. A.; Ruoff, R. S. Carbon-Based Supercapacitors Produced by Activation of Graphene. *Science* **2011**, *332*, 1537–1541.
71. Murali, S.; Quarles, N.; Zhang, L. L.; Potts, J. R.; Tan, Z.; Lu, Y.; Ruoff, R. S. Volumetric Capacitance of Compressed Activated Microwave-Expanded Graphite Oxide (a-MEGO) Electrodes. *Nano Energy* **2013**, *2*, 764–768.
72. Hantel, M. M.; Kaspar, T.; Nesper, R.; Wokaun, A.; Kötz, R. Partially Reduced Graphene Oxide Paper: A Thin Film Electrode for Electrochemical Capacitors. *J. Electrochem. Soc.* **2013**, *160*, A747–A750.
73. Lei, Y.; Huang, Z.; Yang, Y.; Shen, W.; Zheng, Y.; Sun, H.; Kang, F. Porous Mesocarbon Microbeads with Graphitic Shells: Constructing a High-Rate, High-Capacity Cathode for Hybrid Supercapacitor. *Sci. Rep.* **2013**, *3*, 2477–2482.
74. Li, Z.; Xu, Z.; Wang, H.; Ding, J.; Zahiri, B.; Holt, C. M. B.; Tanab, X.; Mitlin, D. Colossal Pseudocapacitance in a High Functionality-High Surface Area Carbon Anode Doubles the Energy of an Asymmetric Supercapacitor. *Energy Environ. Sci.* **2014**, *7*, 1708–1718.
75. Chen, Z.; Yuan, Y.; Zhou, H.; Wang, X.; Gan, Z.; Wang, F.; Lu, Y. 3D Nanocomposite Architectures from Carbon-Nanotube-Threaded Nanocrystals for High-Performance Electrochemical Energy Storage. *Adv. Mater.* **2014**, *26*, 339–345.
76. Gogotsi, Y.; Simon, P. True Performance Metrics in Electrochemical Energy Storage. *Science* **2011**, *334*, 917–918.
77. Hao, L.; Li, X.; Zhi, L. Carbonaceous Electrode Materials for Supercapacitors. *Adv. Mater.* **2013**, *25*, 3899–3904.